Contribution of vertical advection to supergradient wind in tropical cyclone boundary layer: A numerical study

Rong Fei[1,2,3], Yuqing Wang[3,1], and Yuanlong Li[4,3]

[1]State Key Laboratory of Severe Weather, Chinese Academy of Meteorological Sciences, China Meteorological Administration, Beijing, China

[2]College of Earth and Planetary Sciences, University of Chinese Academy of Sciences, Beijing, China

[3]International Pacific Research Center and Department of Atmospheric Sciences, University of Hawaii at Manoa, Honolulu, HI, USA

[4]Ministry of Education Key Laboratory for Earth System Modelling, Department of Earth System Science and Joint Center for Global Change Studies (JCGCS), Tsinghua University, Beijing, China

March 8, 2020 (submitted)
July 28, 2020 (first revision)
October 21, 2020 (second revision)
January 7, 2021 (third revision)
Dateline

Submitted to ***Journal of the Atmospheric Sciences***

* Corresponding author address:
Prof. Yuqing Wang
International Pacific Research Center
University of Hawaii at Manoa
404A/POST, 1680 East West Road,
Honolulu, HI 96822, USA.
Email: yuqing@hawaii.edu

Abstract

The existence of supergradient wind in the interior of the boundary layer is a distinct feature of a tropical cyclone (TC). Although the vertical advection is shown to enhance supergradient wind in TC boundary layer (TCBL), how and to what extent the strength and structure of supergradient wind are modulated by vertical advection are not well understood. In this study, both a TCBL model and an axisymmetric full-physics model are used to quantify the contribution of vertical advection process to the strength and vertical structure of supergradient wind in TCBL. Results from the TCBL model show that the removal of vertical advection of radial wind reduces both the strength and height of supergradient wind by slightly more than 50%. The removal of vertical advection of agradient wind reduces the height of the supergradient wind core by ~30% but increases the strength of supergradient wind by ~10%. Results from the full-physics model show that the removal of vertical advection of radial wind or agradient wind reduces both the strength and height of supergradient wind but the removal of that of radial wind produces a more substantial reduction (52%) than the removal of that of agradient wind (35%). However, both the intensification rate and final intensity of the simulated TCs in terms of maximum 10-m wind speed show little differences in experiments with and without the vertical advection of radial or agradient wind, suggesting that supergradient wind contributes little to either the intensification rate or the steady-state intensity of the simulated TC.

1. Introduction

Tropical cyclones (TCs) are warm-cored cyclonic atmospheric vortices and form over warm tropical oceans. Although to the first order, the wind and mass fields in TCs are in gradient wind balance in the free troposphere, the winds in the boundary layer deviate substantially from the gradient wind balance, and thus are unbalanced, due to the presence of surface friction and vertical turbulent mixing (e.g., Hawkins and Rubsam 1968; Willoughby 1990; Zhang et al. 2001; Bell and Montgomery 2008). The unbalanced flow in the boundary layer is often referred to as agradient winds ($v_a = v - v_g$, where v is tangential wind and v_g is the gradient wind), which includes both subgradient winds in the lower part and supergradient winds in the upper part of the TC boundary layer (TCBL). Previous studies based on both observations and numerical simulations have shown that supergradient winds are much stronger inside the radius of maximum gradient wind (RMGW) than outside the RMGW and also stronger in strong TCs, and can be as large as 10–15% of the gradient winds (Mitsuta et al. 1988; Zhang et al. 2001; Kepert 2006a, b; Schwendike and Kepert 2008; Miyamoto et al. 2014).

In some earlier studies, the weak subsidence in the eye of a TC was considered as a result of the radially outward advection of supergradient air into the eyewall (Malkus 1958; Kuo 1959). This is because once the supergradient winds are transported upward out of the boundary layer by eyewall updraft, an outward agradient force (the sum of the outward Coriolis force and centrifugal force is greater than the inward pressure gradient force) will be induced, which will lead to the development of outflow near the RMGW immediately above the boundary layer, and thus divergence inside the RMGW and subsidence in the eye region. More recently, the supergradient winds are also considered as a momentum source of the eyewall above the boundary layer in a TC when they are advected upward out of the boundary layer by the eyewall updraft (Schmidt and Smith 2016; Montgomery and Smith 2017, 2018). However, whether the upward advection of the supergradient component of boundary layer wind is a major momentum source to the spinup of the eyewall of a TC is still under debate (Willoughby 1991; Zhang et al. 2001; Heng et al. 2017, 2018; Montgomery and Smith 2018; Li et al. 2020a). Nevertheless, the existence of supergradient winds in the interior of the boundary layer is a distinct feature of a TC and may play some important dynamic and thermodynamic roles in TCs. Therefore, understanding the controlling processes of supergradient winds may help improve the understanding of TC dynamics in general and TC boundary layer dynamics in particular.

The earlier theoretical studies relevant to TCBL can be traced back to Rosenthal (1962), Eliassen (1971), and Eliassen and Lystad (1977). These studies presented the Ekman layer of a stationary hurricane-like circular vortex and used the result to explain why the eye with no clouds exists in TCs. Although the presence of supergradient winds was not the foci of these studies, their results indeed showed the existence of weak supergradient winds in the upper part of the Ekman layer. In a depth-averaged (slab) boundary layer model, Shapiro (1983) found that the tangential winds in a small area inside the RMGW in a stationary TC vortex are about 10-15% supergradient, comparable to observations. Such supergradient flow was found to be primarily due to the radially inward transport of absolute angular momentum (AAM), suggesting that the nonlinear radial advection process is important to the development of supergradient flow. Note that although the slab boundary layer model can reproduce the supergradient winds in TCBL, later studies demonstrated that the controlling processes of supergradient winds in the slab boundary layer are quite different from those in a multi-level boundary layer model as demonstrated by Kepert (2010a, b) and Williams (2015). Namely, the radial advection of AAM is important only in the lower part of the boundary layer and vertical advection dominates the radial advection in the upper part of the boundary layer in producing supergradient winds in TCBL.

A more systematic and comprehensive study of supergradient winds in TCBL was given in Kepert (2001) and Kepert and Wang (2001, hereafter KW01). Kepert (2001) extended the earlier linear theory of Ekman layer for a circular vortex to include the effects of TC vortex translation and a more realistic parameter space of TC-like vortices. He found that the linear theory could well capture the radial variation of the TC inflow boundary layer and the height of the maximum in supergradient winds, namely the boundary layer jet in the TC vortex core, but produced only weak supergradient winds as in earlier linear Ekman model. This underestimation of supergradient winds by the linear model was attributed to the strong effect of nonlinearity, in particular the vertical advection process, as demonstrated by KW01 in a multi-level boundary layer model. In KW01, realistic strength of supergradient winds was reproduced in a full nonlinear TCBL model. Results from an AAM budget analysis indicate that above the jet maximum, upward transport of jet momentum by the eyewall updraft becomes important, which is primarily balanced by the spindown due to the radial advection associated with the weak outflow induced by the outward agradient force. As a result, any process that prevents the development of outflow in the upper part of the boundary layer is important to the maintenance of strong supergradient winds. Results from a radial wind budget analysis in KW01 showed that the vertical advection of inflow plays a role in deepening the inflow. As a result, KW01 hypothesized that the upward advection of inflow can partly offset the outflow resulting from the upward advection of supergradient winds in the upper part of the boundary layer. This implies that the upward advection of boundary layer inflow may be important to the maintenance of supergradient winds in the upper part of the TCBL. In a more recent study, Williams (2015) generally confirmed the findings of KW01 and also found that the upward transport of supergradient momentum by both vertical advection and vertical diffusion leads to the production of a supergradient maximum in the upper part of the inflow boundary layer.

The above studies from both KW01 and Williams (2015), as well as Kepert (2010a, b), demonstrate that in addition to the radial inward transport of AAM, vertical advection is also important to the realistic strength and vertical structure of supergradient winds in TCBL. However, results from the AAM and radial wind budgets could not isolate the relative importance of the vertical advection of supergradient winds from the vertical advection of radial winds to the realistic strength and structure of supergradient winds in TCBL. This is because the budget terms based on the full momentum equation(s) already included the feedback from the contribution of vertical advection because vertical advection may change the advected variable(s) and affect the distributions of other variables as well, which in turn may affect other processes, including the vertical advection itself, in the model. This means that the budget analyses only indicated the qualitative importance but could not give quantitative measure of the net contribution. Furthermore, results from TCBL models only provide the steady-state response of the boundary layer to a given distribution of gradient winds at the top of the boundary layer. It is unclear whether those findings are applicable for an intensifying TC and what the consequence of any change in supergradient winds in the boundary layer is to the intensification and maximum intensity of a TC.

In this study, both an axisymmetric TCBL model and an axisymmetric full-physics model are used to address the above issues. We will first examine the sensitivity of the simulated supergradient winds in TC boundary layer to the vertical advection of agradient winds and radial winds in the nonlinear TCBL model. We then reevaluate the findings from the TCBL model in an axisymmetric full-physics model and discuss the possible role of supergradient winds in affecting the simulated TC intensification rate and the maximum intensity as a byproduct. The rest of the paper is organized as follows. The models used and experimental design are described in section 2. Results from the TCBL model and the full-physics model are discussed, respectively, in sections 3 and 4. Our major findings are summarized and discussed in the last section.

2. Models and experimental design

Two axisymmetric numerical models are used in this study: a TCBL model similar to that of KW01 and the latest version (V19.8) of the advanced full-physics cloud model (CM1) developed and used by Bryan and Fritsch (2002) and Bryan and Rotunno (2009). Here, the axisymmetric models are employed because issues we attempted to address are mostly relevant to the axisymmetric dynamics in relatively strong TCs.

a. The TCBL model

The axisymmetric TCBL model used in this study is a multi-level boundary layer model that is used to study the steady-state response of the boundary layer flow to a prescribed pressure gradient force in gradient wind balance with a specified gradient distribution which represents a mature TC vortex (KW01; Williams 2015). The main advantage of using such a “diagnostic” model is that it can capture the basic dynamical feature of the boundary layer flow in response to the prescribed pressure (gradient force) distribution. Therefore, the model can be used to help understand the basic dynamics of the TCBL and also the possible role of boundary layer dynamics in TC structure and intensity changes (e.g., Kepert 2017; Li and Wang 2020a, b). The TCBL model used here is the same as that used in Li and Wang (2020a, b), which is a simplified version of the model used in KW01.

The model includes two momentum equations for tangential and radial winds, respectively, and the continuity equation for incompressible atmosphere. The model has a top at 4-km height and is unevenly discretized into 40 layers between the surface and the model top, with the lowest model level of tangential and radial winds at 10-m height. The model has a radial grid spacing of 1 km and covers the region from the TC center to a radius of 2500 km. The subgrid-scale turbulent mixing is parameterized with the Smagorinsky scheme (Bryan and Rotunno 2009), as used in the full-physics model CM1. The horizontal mixing length (l_h) is set to be 700 m. The vertical mixing length is parameterized as $l_v{}^{-2} = l_\infty{}^{-2} + [\kappa(z + z_0)]^{-2}$ (Bryan et al. 2017), where $\kappa = 0.4$ is the von Kármán constant, z is height, and z_0 is aerodynamic roughness length (set to zero in the TCBL model), and the asymptotic vertical mixing length l_∞ is set to be 70 m. Values of l_h and l_∞ are both inferred from estimates based on observations in TCs (Zhang et al. 2011; Zhang and Montgomery 2012). The surface drag coefficient is a function of 10-m wind speed ($|\overrightarrow{V_{10}}|$) and is given as $C_D = \max\left[(1.0, \min\left(2.4,\ 1.0 + 0.07(\left|\overrightarrow{V_{10}}\right| - 5.0)\right)\right] \times 10^{-3}$. The Coriolis parameter is assumed to be constant at 5×10^{-5} s^{-1}. These are chosen to be the same as those used in the full-physics model discussed in section 2b below so that a direct comparison between the two models can be possible.

Four numerical experiments are performed using the TCBL model. In all experiments, the distribution of pressure gradient force throughout the model domain is prescribed and is in balance with a specified radial profile of gradient wind at the model top, which is obtained from the gradient wind at 2-km height averaged during the quasi-steady state (96–120 h of simulation) from the control experiment using the axisymmetric full-physics model CM1 (CTL_CM1; cf. Table 1) described below. The use of gradient wind from CM1 not only provides a more realistic vortex profile for the TCBL model but also makes the following comparisons of results between the two models more straightforward. In the control experiment (CTL_BL), all default settings as described above are utilized. To determine to what extent the vertical advection of radial and agradient winds may affect the boundary layer flow, three sensitivity experiments are conducted. In these three sensitivity experiments, the vertical advections of radial wind (noU_BL), agradient wind (noVa_BL), and both agradient and radial winds (noUVa_BL) within the radius of 40 km (in inner-core region with supergradient winds) are ignored, respectively. In all TCBL model experiments, the boundary layer achieves a steady state after several hours. All results and budget analyses discussed below are for the steady-state response (after 12 h model run in each experiment). Note that in the TCBL model the pressure gradient wind force is height independent, and thus the vertical shear of gradient wind is zero. As a result, the vertical advection of agradient wind also represents the vertical advection of total tangential wind, which is different from the full-physics model experiments where gradient wind decreases with height in general.

Four extra TCBL model experiments are also performed. In these experiments, instead of using the radial gradient wind profile at 2-km height, the actual radial-vertical distributions of gradient winds averaged during the quasi-steady stage in the corresponding full-physics CM1 experiments (CTL_CM1, noU_CM1, noVa_CM1, and noUVa_BL) are used, namely CTL_2d_BL, noU_2d_BL, noVa_2d_BL, and noUVa_2d_BL (see Table 1), as done in Stern et al. (2020). These four experiments are conducted to help understand the differences in the simulated supergradient winds between the TCBL model and the full-physics model CM1 as described below, as well as provide a direct assessment to see how accurate of the boundary layer model in reproducing the boundary layer structure in full-physics model simulations. Note that the results from these extra experiments are discussed in section 4 after the results from the full-physics model CM1 experiments are discussed and when the differences between the TCBL and CM1 are explained.

b. The full-physics model (CM1)

The full-physics model used in this study is the axisymmetric version of the nonhydrostatic and fully-compressible cloud model CM1 developed by Bryan and Fritsch (2002). Instead of the steady-state response of the boundary layer flow to prescribed pressure gradient force in the TCBL model described in section 2a, the full-physics model allows a full interaction between the free atmosphere and the boundary layer. This means that the boundary layer response can in turn affect the pressure gradient force and gradient wind above the boundary layer. As a result, on one hand, the similarity and difference in the boundary layer structure in the two models can be examined, and on the other hand, the possible feedback of the boundary layer response to TC structure and intensity change can be recognized. Since a full description of CM1 can be found in Bryan and Fritsch (2002) and Bryan and Rotunno (2009), only some key features relevant to this study are briefly summarized here.

The model domain size is 3100 km (radial) × 25 km (vertical). The radial grid spacing is 1 km in the inner-core region and is stretched to 14 km to the radial outer boundary. The model has 59 vertical levels and the vertical grids are stretched below 5.5 km as that done in Li et al. (2019). The Thompson microphysical scheme (Thompson et al. 2008) is applied for moist cloud microphysics. No cumulus convective parameterization is used in all experiments. The subgrid-scale turbulent mixing is also parameterized by the Smagorinsky scheme (Bryan and Rotunno 2009) and the same horizontal and vertical mixing lengths are utilized as in the TCBL model. Note that our preliminary tests show that the main conclusions of this study are not dependent on the values of the vertical and horizontal mixing lengths in reasonable ranges in the TCBL model or in CM1. Therefore, only analyses based on the default values mentioned above are discussed hereafter. The surface drag coefficient is a function of 10-m wind speed, which is also the same as that used in the TCBL model as described in section 2a, and the surface exchange coefficient for enthalpy is set to be a constant of 1.2×10^{-3}. The Newtonian cooling capped at 2 K day^{-1} is introduced to mimic radiative cooling (Rotunno and Emanuel 1987).

The moist tropical sounding of Dunion (2011) is adopted as the unperturbed environment of the model tropical atmosphere. Sea surface temperature is fixed at 29°C, and an *f*-plane is assumed with the Coriolis parameter of 5×10^{-5} s^{-1}. The initial TC vortex has the radial distribution of tangential wind following that introduced by Wood and White (2011) with the initial maximum tangential wind speed of 15 m s^{-1} at a radius of 80 km from the vortex center. The radial shape parameter is set to be 1.6 and the tangential wind speed decreases linearly with height to zero at a height of about 18 km. To address whether and to what extent the vertical advection influences the strength and structure of supergradient winds in the boundary layer, and the TC intensification rate and maximum intensity, four experiments are conducted using CM1 as done in the TCBL model. In the control experiment (CTL_CM1), all default model settings described above are adopted. In the three sensitivity experiments, the vertical advections of radial winds (noU_CM1), agradient winds (noVa_CM1), and both radial and agradient winds (noUVa_CM1) are removed below 3-km height and within the radius of 40 km (in the inner-core region) after 48 hours (spinup period), respectively. The first 48-h integration is considered as the spinup of model boundary layer dynamics and model physics. Since our interest is the boundary layer dynamics after the model TC develops a typical eyewall and boundary layer structure in the primary intensification and the quasi-steady evolution stages, the removal of vertical advection term is activated after the initial 48-h adjustment. Note that only the vertical advection term below 3-km and within the radius of 40 km is removed in all sensitivity experiments so that its dynamical effect is mainly constrained in the inner-core region of the TCBL.

To reduce the effect of model internal variability and ensure the robustness of the model results, ensemble simulations with 21 members for each experiment are performed, similar to those in Xu and Wang (2018) and Li et al. (2020a). Besides the standard run described above, in the remaining

20 runs, the initial maximum tangential wind speed is perturbed by increments of ±0.1 m s^{-1} (for 10 runs) and the radius of maximum wind is perturbed by increments of ±0.4 km (for 10 runs). All 21 runs for each experiment are integrated for 120 h with every 6-min model output for the composite analyses discussed in section 4. In the following analyses, only results of the ensemble composite from the 21 runs for each experiment are discussed. Our preliminary tests indicate that the main conclusions from this study are not affected by the perturbation increments in reasonable ranges.

In addition, we should point out that by turning off the vertical advection in this study, we have not only suppressed the direct contribution of vertical advection but also suppressed any possible feedback from the indirect effect of vertical advection on other processes, including the vertical advection of the variable itself. Note also that the vertical advection is removed only in the inner core boundary layer, namely in the region with considerable supergradient wind component. As a result, except for changes to the wind structure in the inner core boundary layer, the overall TC structure is nearly unchanged in the full-physics model experiments (see discussion in section 4), which also justifies the adequacy of the methodology used for the purpose to address an issue locally in the inner core boundary layer. We should also remind that the model system with vertical advection artificially removed does not exist in the real word. Therefore, the thought (sensitivity) experiments should not be considered as “realistic” simulations but are specially designed to explore the relative contribution of vertical advection(s) to the boundary layer supergradient wind in a sophisticated nonlinear system. Note that a similar approach was also recently used in Li et al. (2020a) and some extended discussions on the method can be found in Li et al. (2020b).

3. Results from the TCBL model

Figure 1 compares the radius-height cross-sections of total tangential wind (v) and its agradient wind component ($v_a = v - v_g$) in experiments CTL_BL, noU_BL, noVa_BL, and noUVa_BL. We can see that in CTL_BL (Fig. 1a), there is a maximum wind speed of more than 80 m s^{-1} at the height between 500 and 1000 m, accompanied by a maximum supergradient wind at 550-m height slightly inside the radius of maximum tangential wind (RMW). The maximum supergradient wind reaches 19 m s^{-1}, which is about 25% of the maximum tangential wind speed in the boundary layer. In addition to supergradient wind, a region with weak subgradient wind slightly over 6 m s^{-1} appears right above the supergradient wind region near the RMW. This is associated with inertial oscillation related to the rotating flow in the boundary layer (Kepert 2001; KW01; Rotunno and Bryan 2012; Rotunno 2014; Stern et al. 2020).

The removal of vertical advection of radial wind in noU_BL (Fig. 1b) leads to a substantial reduction of supergradient winds by 54% and a decrease of 52% in the height of the supergradient wind core in the boundary layer (Fig. 2). This suggests that the upward advection of boundary layer inflow plays an important role in deepening and strengthening the supergradient wind core. This occurs because the upward advection of inflow can reduce the outflow induced by the outward agradient force associated with the upward advection of supergradient wind. The removal of vertical advection of agradient wind in noVa_BL (Fig. 1c) also lowers the supergradient wind core by 30% but leads to a strengthening of supergradient wind by 11% (Fig. 2). This implies that the vertical advection of agradient wind plays a role in deepening the supergradient core but somewhat reduces the strength of supergradient wind. This is consistent with the momentum budget analysis presented in Williams (2015), who found that the vertical advection of tangential momentum plays an important role in maintaining supergradient wind in the upper part of the TC boundary layer. The removal of vertical advections of both radial wind and agradient wind in noUVa_BL (Fig. 1d) reduces the strength of the supergradient wind core by 39% and lowers the supergradient core by 53% (Fig. 2). These results demonstrate that it is the vertical advection of radial inflow that substantially enhances supergradient wind, in support to the hypothesis of KW01 based on momentum budget analysis, while the vertical advection of agradient wind deepens the supergradient wind in the boundary layer but moderately reduces the strength of the supergradient wind core, consistent with the result of Williams (2015). Furthermore, in contrast to that in CTL_BL, no obvious subgradient winds occur above the supergradient wind in the three sensitivity experiments, suggesting that the removal of vertical advection of agradient wind, or radial wind, or both would largely suppress the inertial oscillation near the RMW above the TC boundary layer.

Since supergradient wind is closely related to the inward transport of AAM and thus the boundary layer inflow, to understand the differences in supergradient wind in the four experiments discussed above, we show in Fig. 3 the vertical-radial cross-sections of radial wind and agradient force in the four experiments. The agradient force is the imbalance between Coriolis force, centrifugal force, and pressure gradient force, and has the following form in our TCBL model:

$$Agr = fv + \frac{v^2}{r} - (fv_g + \frac{v_g^2}{r}), \quad (1)$$

where f is Coriolis parameter, r is radius, v and v_g are the actual tangential wind and the tangential wind in gradient wind balance with the prescribed pressure gradient force. Namely, the pressure gradient force is represented as the Coriolis force and centrifugal force associated with gradient wind in (1). In CTL_BL (Fig. 3a), there is a strong outflow right above the inflow layer with a maximum outflow over 12 m s^{-1}, which is also found in some observations (Kepert 2006a, b) and numerical models (KW01; Williams 2015). This outflow develops as a response to the outward agradient force due to the upward advection of supergradient wind from below by the eyewall upward motion (e.g., Li et al. 2020a). Akin to that in CTL_BL, the outflow also exists in noU_BL, but is much weaker, with the maximum outflow of 8 m s^{-1} (Fig. 3b). This weaker outflow above the inflow boundary layer can be attributed to the weaker outward agradient force because of weaker supergradient wind in the boundary layer and thus smaller upward advection of supergradient wind in noU_BL than in CTL_BL. In sharp contrast, although the supergradient winds are stronger in noVa_BL (Fig. 1c) than in CTL_BL (Fig. 1a), the outflow aloft in the former is rather weak, only about 4 m s^{-1} (Fig. 3c). This is mainly because without the upward advection of agradient wind in noVa_BL, the flow in the upper part of the boundary layer is nearly in gradient wind balance. As a result, the agradient force above the inflow boundary layer, which is responsible for the development of the outflow layer, is quite small (Fig. 3c). In lack of outflow, the subgradient winds above the inflow boundary layer in CTL_BL (Fig. 3a) also become much smaller in noVa_BL than in CTL_BL (Fig. 3c). Similar to noU_BL, noUVa_BL also exhibits weak agradient force with weak outflow located right above, but the outflow in noUVa_BL is weaker than in noU_BL because of further removal of vertical advection of agradient wind in noUVa_BL (Figs. 3b and 3d). This further confirms that both the strength and height of supergradient wind are largely controlled by the vertical advection of radial wind while the height of supergradient wind and the outflow immediately above the inflow boundary layer are largely controlled by the upward advection of supergradient wind.

To understand the differences in the simulated boundary layer structure in the four experiments, we performed budget analyses of AAM ($= rv + \frac{1}{2}fr^2$)and radial wind, as done in KW01 and Williams (2015). The AAM and radial wind tendency equations in the axisymmetric TCBL model can be written as

$$\frac{\partial(AAM)}{\partial t} = -u\frac{\partial(AAM)}{\partial r} - w\frac{\partial(AAM)}{\partial z} + F_{AAM}, \tag{2}$$

$$\frac{\partial u}{\partial t} = Agr - u\frac{\partial u}{\partial r} - w\frac{\partial u}{\partial z} + F_u. \tag{3}$$

where u and w are radial and vertical velocity, respectively. Terms on the lhs of Eqs. (2) and (3) are local tendencies of AAM and radial velocity, respectively. Note that the tendency of AAM can been understood as the tendency of tangential wind in some sense. Terms on the rhs of (2) are radial advection, vertical advection (vb_vadv), and diffusion (vb_diff, namely F_{AAM}, which contains both horizontal and vertical diffusion including the effect of surface friction) of AAM. Terms on the rhs of (3) are the agradient force [ub_agr, see Eq. (1)], horizontal advection (ub_hadv), vertical advection (ub_vadv), and diffusion (ub_diff, namely F_u, which contains both horizontal and vertical diffusion including the effect of surface friction) of radial velocity. Since we mainly focus on the steady response of the boundary layer to the prescribed pressure gradient force, the local tendencies on the lhs of (2) and (3) are equal to zero. As a result, the balance in the steady-state solution of the TCBL model varies among different processes in the four experiments.

Since our main interest is in the supergradient wind, the vertical profiles of tendencies at 17 km radius, which is near the radius of maximum supergradient wind in CTL_BL (Fig. 1a), are discussed herein. We first look at the vertical profiles of tangential and radial winds at 17 km radius (Fig. 4a). The inflow in CTL_BL is the strongest among the four experiments and the depth of the inflow layer reaches 750 m above the surface, slightly above the maximum in supergradient wind (at about 600 m). In noU_BL, the depth of the inflow layer becomes shallower in accordance with the lower height of the maximum in supergradient wind than in CTL_BL. In contrast, in noVa_BL, although the supergradient wind is largely suppressed in the upper part of the boundary layer, the depth of the inflow layer is almost the same as that in CTL_BL. In noUVa_BL, the height of supergradient wind is also reduced in accordance with the lowering of inflow depth as described for noU_BL above. These results indicate that the removal of vertical advection of radial wind reduces the height of supergradient wind core by lowering the inflow depth while the removal of vertical advection of agradient wind lowers the supergradient wind core by redistributing the supergradient wind in the vertical.

Figures 4b-d compare the vertical profiles of AAM tendencies due to all three terms on the rhs of Eq. (2) near the radius of maximum supergradient wind among all four experiments. In CTL_BL, below the level of supergradient wind maximum, the positive AAM tendency contributed by inward advection (Fig. 4b) is balanced by vertical advection and diffusion terms (Figs. 4c and 4d). Above the level of supergradient wind maximum, the positive vertical advection of AAM is balanced by the radially outward transportation of AAM associated with outflow and diffusion, which is negative below 1000-m height and becomes positive but very small above. Note that the positive contribution by the inward advection of AAM reaches a height about 100 m above the level of supergradient wind maximum. This is mainly caused by the upward advection of inflow from below, which largely balances the negative radial wind tendency due to diffusion, indicating that the upward advection of inflow plays an important role in deepening and strengthening supergradient wind. This is indeed supported by the weaker strength and shallower depth of supergradient wind in noU_BL than in CTL_BL (Fig. 4a). The negative vertical advection of AAM below the level of supergradient wind maximum in CTL_BL and its lack in noVa_BL (Fig. 4c) explains why the tangential (supergradient) wind is stronger below 500 m height in noVa_BL than in CTL_BL (Fig. 4a). In noUVa_BL, the positive tendency due to inward advection of AAM is balanced by the negative tendency due to diffusion (mainly vertical diffusion) in the lower part of the boundary layer. In this case, supergradient wind appears at the lowest layer among the four experiments. The budget results indicate that the inward advection of AAM, and thus the boundary layer inflow, is the initial forcing to the development of supergradient wind in the lower part of the boundary layer while vertical advection, in particular the vertical advection of radial wind, is responsible for the deepening and further strengthening of supergradient wind in the upper part of the boundary layer.

To understand the maintenance of radial wind in the four experiments, we show in Fig. 5 all terms on the rhs of Eq. (3). We can see that in all four experiments (Fig. 5a), the agradient force above the surface layer is positive, and thus tends to decelerate the inflow in the layer where supergradient winds are located. The weak inward agradient force further above the outward agradient force is related to the subgradient wind as mentioned earlier, which is the largest and appears at the highest level in CTL_BL but is negligible in both experiments without the vertical advection of radial wind (namely in noU_BL and noUVa_BL). The radial advection dominantly contributes to the acceleration of inflow below the height of supergradient wind maximum but becomes very small above (Fig. 5b). In both CTL_BL and noVa_BL, the vertical advection of radial wind is negative and thus plays a role in deepening the inflow or weakening the outflow above the inflow boundary layer (Fig. 5c). Therefore, the vertical advection of radial wind largely offsets the outflow induced by the outward agradient force and thus holds supergradient wind in a deeper layer, as pointed out by KW01. The positive diffusion (mainly vertical diffusion) in the lower boundary layer, which decreases with height rapidly, results from surface friction and represents the frictional deceleration of inflow (Fig. 5d). Further above, the diffusion becomes negative but relatively small, partly contributing to the deepening of the inflow layer. The above budget results explain well why the inflow layer is shallower and supergradient wind is weaker in both noUVa_BL and noU_BL than in CTL_BL and noVa_BL (Fig. 4a).

4. Results from the full-physics model

Results discussed in section 3 are the steady-state response of the boundary layer flow to the prescribed height-independent pressure gradient force in gradient wind balance above the boundary layer. We have found that the vertical advection of radial wind is key to both the strength and height of supergradient wind in TCBL and the vertical advection of agradient wind deepens supergradient wind while slightly reduces the strength of supergradient wind. It is our interest in this section to see the extent to which the findings based on the boundary layer model may apply to a full-physics model in which the pressure gradient force is no longer prescribed. This means that the boundary layer response may in turn affect the pressure distribution. Therefore, in addition to confirm results from the TCBL model, the differences in the simulated TC structure and intensity between the control experiment (with all default model settings in CTL_CM1) and sensitivity experiment with the vertical advection of radial wind or agradient wind, or both ignored can also help address whether and to what extent supergradient wind may affect the intensification rate and final steady-state intensity of the simulated TC.

Figure 6 compares the temporal evolutions of the ensemble mean maximum 10-m height wind speed and maximum supergradient wind in CTL_CM1, noU_CM1, noVa_CM1, and noUVa_CM1. Since the removal of vertical advection term in each sensitivity experiment is activated after 48-h spinup, our analyses will focus on the results after 48-h simulations. We can see from Fig. 6a that the removal of the vertical advection of radial wind or agradient wind or both produces negligible changes to both the overall intensification rate during the primary intensification period from 48 to 72 h of simulation and the final intensity in the quasi-steady stage of the simulated storm. However, the differences in the evolution of supergradient wind among the four experiments increase with time as the storms are intensifying and reach the maximum after 96 h of simulations when the storms start experiencing their quasi-steady evolutions (Fig. 6b). The supergradient wind develops most slowly in noUVa_CM1 among all four experiments (see also Fig. 2). As a result, the maximum supergradient wind averaged during the quasi-steady stage (96-120 h of simulation) in noUVa_CM1 is reduced by 59% compared to that in CTL_CM1. The strength of supergradient wind in noU_CM1 is reduced by 52% compared to that in CTL_CM1, which is slightly stronger than that in noUVa_CM1. The removal of vertical advection of agradient wind in noVa_CM1 reduces maximum supergradient wind by 35%, which is the smallest reduction among the three sensitivity experiments in CM1. Although most of the results from CM1 are qualitatively and quantitatively consistent with those in the TCBL model, the removal of vertical advection of agradient wind leads to 11% increase in the strength of supergradient wind in the TCBL model while it results in a reduction of 35% in CM1 (Fig. 2). To understand the similarities and differences in the simulated supergradient winds and TC intensity among these experiments and the related physical processes, we choose the quasi-steady stage from 96 to 120 h of simulations for further analyses. Note that the major conclusions based on the results for the intensification stage (from 48 to 96 h) are consistent with those for the quasi-steady stage discussed below (not shown).

The overall structures of the simulated TCs in their quasi-steady stages are very similar in CTL_CM1, noU_CM1, noVa_CM1, and noUVa_CM1 except for the differences below about 3-km height in the inner-core region where vertical advections are modified (Fig. 7). The distinct differences in the three sensitivity experiments from the control experiment CTL_CM1 are closely related with the weaker supergradient wind and the associated shallower and weaker outflow layer immediately above the inflow boundary layer in the inner core. This indicates that the removal of vertical advection of radial or agradient wind or both below 3-km height mainly has a local impact by suppressing the boundary layer supergradient wind and its related outflow above the inflow boundary layer. However, this local effect on the boundary layer supergradient wind has little impact on the overall structure (Fig. 7) of the simulated storm, the overall intensification rate, and the final storm intensity (Fig. 6). Since the substantial reduction of supergradient wind in the boundary layer in the three sensitivity experiments largely reduces the upward advection of supergradient wind from the boundary layer, our results imply that the upward advection of supergradient wind out of the boundary layer should not be a major process of the overall TC intensification. This is in support to the hypothesis of Heng et al. (2018), who indicated that the upward advection of supergradient wind out of the boundary layer might contribute little to TC intensification because its spinup of tangential wind is almost balanced by the spindown due to the related outflow. This has also been recently demonstrated by Li et al. (2020a), who showed that the upward advection of supergradient wind from the boundary layer has little effect on the intensification of the simulated TC but slightly increased the TC quasi-steady intensity. However, our results contrast with the claim of Schmidt and Smith (2016) and Montgomery and Smith (2017, 2018), who stated that it is the upward advection of tangential momentum associated with supergradient wind in the boundary layer that spins up the tangential wind aloft in the eyewall. This point will be further discussed later.

Figure 8 shows the time-averaged tangential wind and agradient wind during the quasi-steady stage in the four CM1 experiments. Generally, the strength and structure of boundary layer winds in CTL_CM1 (Fig. 7a) are similar to those in CTL_BL (Fig. 1a) except for the slightly weaker subgradient wind above 2 km height in CTL_CM1. This is mainly because the pressure gradient force in the TCBL model, which is taken from that at 2-km height from CTL_CM1, is height-independent, while it is height-dependent and decreases with height in CTL_CM1. As a result, the upward advection of gradient wind in CTL_CM1 slightly reduces the subgradient wind above the boundary layer in CTL_CM1. However, in the supergradient wind region, the upward advection of gradient wind may lead to a weak outward agradient force and thus the development of outflow, contributing negatively to supergradient wind. To verify the above hypothesis, an additional simulation (labeled as CTL_2d_BL in Table 1) is conducted, in which the 2-dimensional (radial-vertical) pressure gradient force averaged in the quasi-steady state during 96–120 h of simulation in CTL_CM1 is used to drive the TCBL model instead of that at 2-km height used in CTL_BL. As expected, in CTL_2d_BL (Fig. 9a) the maxima in subgradient wind above the boundary layer and supergradient wind in the boundary layer are both slightly reduced while the height of the supergradient wind core is slightly increased compared with those in CTL_BL (Fig. 2), leading to the distribution of agradient wind from the TCBL model more consistent with that in CTL_CM1 (Fig. 8a).

With the vertical advection of radial wind removed in noU_CM1, the supergradient wind is reduced by 52%, close to that of 54% in noU_BL, and the height of the supergradient wind core is lowered by 69% compared with that in CTL_CM1, which is larger than the reduction of 52% in noU_BL relative to CTL_BL in the TCBL model (Fig. 8b and Fig. 2). This difference in the height of the supergradient core is found to be largely related to the difference in the radial and vertical distribution in gradient wind between noU_BL and noU_CM1 because the gradient wind can be changed in response to changes in the boundary layer flow in noU_CM1. This is verified by results from the experiment noU_2d_BL (Table 1, Fig. 9b) in which the TCBL model is driven by the two-dimensional pressure gradient force from noU_CM1. In addition, consistent with that in noU_BL discussed in section 3 (Fig. 1b), there is no distinct subgradient wind above the supergradient wind because of the weak agradient force related to the vertical advection of weak supergradient wind from the boundary layer in noU_CM1 (Fig. 8b) and noU_2d_BL (Fig. 9b).

The removal of vertical advection of agradient wind in noVa_CM1 leads to a reduction of supergradient wind by around 35% and a reduction of the height of the supergradient wind core by 51% of that in CTL_CM1 (Fig. 8c and Fig. 2). This is not fully consistent with the results in the TCBL model in which the removal of vertical advection of agradient wind leads to a 11% increase in the strength of supergradient wind and a reduction of the height of the supergradient core by only 30% (Figs. 1c and 2). The difference is mainly due to the difference in the radial and vertical distributions in gradient wind between noVa_BL and noVa_CM1 as discussed above for noU_CM1. This is confirmed by the results in noVa_2d_BL (Fig. 9c). Now compared with that in CTL_2d_BL, the strength and the height of the supergradient wind core are reduced by 32% and 50%, respectively, both are close to those in noVa_CM1 relative to CTL_CM1 (Fig. 2). In addition, we also conduct an extra experiment in which the radial and vertical distribution of gradient wind averaged during the quasi-steady stage from noVa_CM1 is used to drive the TCBL model with vertical advection of both radial and agradient wind, the results (figure not shown) show no increase in the strength of the supergradient wind core compared to that in noVa_2d_BL. This confirms that the difference in response to the removal of vertical advection of agradient wind in the TCBL model and CM1 results primarily from the difference in the gradient wind as will be discussed further below. Note that Li et al. (2020a) found a ~35% reduction in the strength of supergradient wind by the removal of the positive upward advection of supergradient wind from the boundary layer but little effect on the intensification rate of their simulated storm.

The removal of vertical advections of both radial wind and agradient wind in noUVa_CM1 reduces the strength of supergradient wind by 59% and the height of the supergradient wind core by 69% from that in CTL_CM1 (Figs. 8a and 8d and Fig. 2). The reduction in both the strength and height in the supergradient wind core in noUVa_CM1 seems to be dominantly contributed by the removal of vertical advection of radial wind, as found in the TCBL model discussed in section 3. However, both reductions are larger than those (39% and 53%) in the TCBL model (Fig. 2). As in noU_CM1 and noVa_CM1, the larger reductions in CM1 result primarily from the difference in the radial and vertical distributions in gradient wind between the TCBL model and CM1. This is also verified by the results from the experiment noUVa_2d_BL (Fig. 9d and Fig.2). In addition, similar to the results from the TCBL model discussed in section 3, no obvious subgradient wind appears above the supergradient wind in all three sensitivity experiments in CM1 (Fig. 8) and their corresponding boundary layer model (Fig. 9), which is in sharp contrast to that in CTL_CM1 in which subgradient wind of over 4 m s^{-1} appears in the inner core above 2-km height (Fig. 8a).

Figure 10 compares the low-level radial wind and agradient force[1] averaged during the quasi-steady stage in the four experiments in CM1. We can see that the major features of radial wind and agradient force in the four CM1 experiments are similar to those in the TCBL model except that the agradient force in noVa_CM1 is smaller than that in noVa_BL (Figs. 3c and 10c) because of the upward advection of weaker supergradient wind in the former (Figs. 1c and 8c). The stronger outflow layer immediately above the inflow layer in CTL_CM1 is likely responsible for the more outward tilt of the RMW in the lower troposphere than in the other three sensitivity experiments in CM1 (Fig. 8). This is different from that in the TCBL model where the pressure gradient force is

---

[1] Note that in CM1, the agradient force has the form $Agr = fv + \frac{v^2}{r} - c_p\theta_v\frac{\partial \pi'}{\partial r}$, where c_p is the specific heat at constant pressure of dry air, θ_v is the virtual potential temperature, π' is the perturbation Exner function and the others are the same as that in Eq. (1).

prescribed and height-independent. In this sense, in the full-physics model, in addition to changes in supergradient wind and its related outflow aloft in the inner core, the removal of vertical advection of radial wind and/or agradient wind also leads to some changes in the inner-core structure to the simulated storm likely through modifying eyewall convection and thus diabatic heating as discussed further below although the overall structure remains similar to that in CTL_CM1 (Fig. 7).

We have mentioned above the changes in gradient wind in the full-physics model simulations using CM1 and attributed some differences between the TCBL model discussed in section 3 and CM1 to the response of gradient wind to the removal of vertical advection of radial wind and/or agradient wind. Therefore, we further examine how the balanced gradient winds and eyewall diabatic heating in the sensitivity experiments are changed due to the removal of vertical advection of radial wind and/or agradient wind compared to that in CTL_CM1. Figure 11 compares the radius-height cross sections of gradient winds and diabatic heating rate averaged during the quasi-steady stage in the four CM1 experiments. Note that both the radial locations of the maximum total tangential wind speed (RMW) and the maximum gradient wind speed (RMGW) are also shown in Fig. 11 for a reference. Although the strength of supergradient wind varies up to ~60% among the four experiments (Fig. 2), the maximum gradient wind speeds are quite similar. The maximum gradient wind is ~5% stronger in noU_CM1 than in other three experiments (Fig. 11).

An interesting result is the difference in the distance between RMGW and RMW (which can be represented by RMGW/RMW, i.e., the ratio of RMGW to RMW) among the four experiments. RMGW/RMW is the largest in CTL_CM1 compared to other experiments, and it also shows large vertical variability in CTL_CM1. The largest RMGW/RMW in CTL_CM1 is closely related to the strongest outflow layer above the inflow boundary layer (Fig. 10a) while the smallest RMGW/RMW in noUVa_CM1 is closely related to the weakest outflow above the inflow boundary layer (Fig. 10d). Since the strength of the outflow layer is largely controlled by the upward advection of supergradient wind out of the boundary layer, it is not surprising that the RMGW/RMW in the lower troposphere is larger in the two experiments (CTL_CM1 and noU_CM1) with vertical advection of agradient wind than that in the two experiments (noVa_CM1 and noUVa_CM1) with the vertical advection of agradient wind ignored (Figs. 8 and 11). Note that the RMGW and RMW show larger departure from each other in CTL_CM1 but very close to each other in the three sensitivity experiments. In addition, the RMW in CTL_CM1 also shows a zigzag change with a large outward tilt below 2 km height and then shift inward and then tilts outward with height again above about 4 km height (Fig. 11a). This change in the RMW is closely related to the changes in agradient winds or inertial oscillation in the eyewall associated with in the rotating boundary layer as recently discussed by Stern et al. (2020). Since the inertial oscillation is largely suppressed in the three sensitivity experiments, the change of RMGW/RMW with height is much smoother than that in CTL_CM1 (Fig. 11). The large outward tilt of the RMGW/RMW in the boundary layer and lower troposphere is closely related to the strong outflow layer above the inflow boundary layer (Fig. 10).

The outflow in CTL_CM1 also leads to relatively weaker vertical motion in the outwardly tilted eyewall and thus weaker diabatic heating in the eyewall than in the three sensitivity experiments (Figs. 7 and 11). Indeed, the weaker gradient wind in CTL_CM1 can be explained by the weaker vertical motion, which results mainly from the stronger outflow (Fig. 10) associated with the upward advection of stronger supergradient wind from the boundary layer as discussed above. The diabatic heating rate in the eyewall (Fig. 11) is roughly proportional to upward motion in the eyewall (Fig. 7). The mid-level diabatic heating rate is smaller and the balanced gradient wind is weaker in CTL_CM1 than in the three sensitivity experiments (Fig. 11). Note that the maximum total tangential wind speed in the lower part of the boundary layer (near the surface) are similar because of the large compensation of weaker gradient wind by stronger supergradient wind in CTL_CM1. As a result, the simulated storm intensification rates and the quasi-steady intensities are very similar in the four experiments. Nevertheless, the presence of supergradient wind might contribute negatively to eyewall convection due to the outflow immediately above the boundary layer, which may slightly weaken the eyewall updraft and causes a larger outward tilt of the eyewall in the lower troposphere.

5. Conclusions and discussion

The unbalanced flow, including both supergradient and subgradient winds or in general agradient wind, in the frictional boundary layer is a distinct feature of a TC in its entire lifetime. The importance of supergradient wind in affecting the reduction factor of low-level wind to surface wind in TCs has been demonstrated in previous studies (e.g., Kepert 2001; 2006a, b; KW01). KW01 found that the nonlinear vertical advection substantially enhances supergradient wind in TCBL. In this study, both an axisymmetric TCBL model and an axisymmetric full-physics model are used to conduct numerical sensitivity experiments to further understand the effect of vertical advection on supergradient wind in TC boundary layer and the possible impact of supergradient wind on the simulated TC intensification and maximum intensity.

Results from the TCBL model demonstrate that supergradient wind in the lower part of the boundary layer results mainly from the inward advection of AAM but both the strength and height of the supergradient wind core are largely controlled by the vertical advection of both radial and agradient winds. We found that the vertical advection of agradient wind deepens supergradient wind in the boundary layer but slightly reduces the strength of supergradient wind. However, the vertical advection of radial wind is key to both the strength and height of supergradient wind in TCBL, which can contribute over 50% to the strength and height of supergradient flow in the boundary layer. This is because the vertical advection of radial wind deepens the inflow layer to against the outward agradient force caused by the upward advection of supergradient wind from below, thus deepening and maintaining strong supergradient wind. The vertical advection of agradient wind also is key to the development of an outflow layer immediately above the inflow boundary layer. The strength and height of the outflow layer are largely determined by the strength and height of supergradient wind in the boundary layer.

Results from the full-physics model CM1 confirm the key role of vertical advection in controlling the strength and height of supergradient wind in TCBL as found in the boundary layer model. The removal of vertical advection of radial wind in CM1 also leads to ~50% reduction of the strength of supergradient wind and even a larger (69%) reduction of the height of supergradient wind in the boundary layer, generally consistent with the results obtained in the TCBL model. The removal of vertical advection of agradient wind leads to 35% reduction of the strength of supergradient winds, which is different from the weak increase in the TCBL model. The differences between the two models are well explained by changes in the strength and distribution of gradient wind simulated in CM1. We also found that the outflow immediately above the inflow boundary layer due to the upward advection of supergradient wind out of the boundary layer can lead to a more outward tilt of the RMW and also slightly weaken eyewall updraft (convection), and thus reducing the diabatic heating rate in the eyewall. This may lead to up to 5% reduction of gradient wind in the balanced response to eyewall heating.

Results from CM1 experiments also show that although supergradient wind (and thus its vertical advection) is largely suppressed in the experiment with the vertical advection of radial wind, or agradient wind, or both artificially removed, both the intensification rate and final intensity in terms of the maximum 10-m wind speed are little affected. This suggests that the upward advection of supergradient wind out of the boundary layer could not be a major process contributing to the overall TC intensification. This supports the hypothesis of Heng et al. (2018) and the recently findings of Li et al. (2020a) but does not support the statement made in Montgomery and Smith (2017, 2018). However, the boundary layer dynamics is key to TC development by modifying the strength and radial location of eyewall updraft inside the RMGW as proposed by Kepert (2017) based on results from a boundary layer model and demonstrated by Li and Wang (2020a, b) based on results from three-dimensional full-physics model simulations. Therefore, results from this study together with those in Li et al. (2020a) and Li and Wang (2020a, b) strongly suggest that more efforts should be given to further understand how the boundary layer dynamics control convection and diabatic heating in the eyewall of a TC in future studies. In addition, we have restricted ourselves on the axisymmetric processes in this study. The conclusions thus may be applicable to quasi-axisymmetric stage of TCs. We plan to conduct three-dimensional simulations to examine how our results/conclusions could be extended into more general three-dimensional TCs in a future study.

Acknowledgments: This study has been supported in part by the National Natural Science Foundation of China under grant 41730960, and in part by the NSF grant AGS-1834300. R. Fei is funded by China Scholarship Council (File 201905330037).

References

Bell, M. M., and M. T. Montgomery, 2008: Observed structure, evolution, and potential intensity of category 5 Hurricane Isabel (2003) from 12 to 14 September. *Mon. Wea. Rev.*, **136**, 2023–2046, https://doi.org/10.1175/2007MWR1858.1.

Bryan, G. H. and J. M. Fritsch, 2002: A benchmark simulation for moist nonhydrostatic numerical model. *Mon. Wea. Rev.*, **130**, 2917–2928, https://doi.org/10.1175/1520-0493(2002)130<2917:ABSFMN>2.0.CO;2.

Bryan, G. H. and R. Rotunno, 2009: The maximum intensity of tropical cyclones in axisymmetric numerical model simulations. *Mon. Wea. Rev.*, **137**, 1770–1789, https://doi.org/10.1175/2008MWR2709.1.

Bryan, G. H., R. P. Worsnop, J. K. Lundquist, and J. A. Zhang, 2017: A simple method for simulating wind profiles in the boundary layer of tropical cyclones. *Bound.-Layer Meteor.*, **162**, 475-502, https://doi.org/10.1007/s10546-016-0207-0.

Dunion, J. P., 2011: Rewriting the climatology of the tropical North Atlantic and Caribbean Sea atmosphere. *J. Climate*, **24**, 893–908, https://doi.org/10.1175/2010JCLI3496.1.

Eliassen, A., 1971: On the Ekman layer in a circular vortex. *J. Meteor. Soc. Japan*, **49**, 784–789.

Eliassen, A., and M. Lystad, 1977: The Ekman layer of a circular vortex: A numerical and theoretical study. *Geophys. Norv*., **31**, 1-16.

Hawkins, H. F., and D. T. Rubsam, 1968: Hurricane Hilda, 1964: II. Structure and budgets of the hurricane on October 1, 1964. *Mon. Wea. Rev.,* **96,** 617–636. https://doi.org/10.1175/1520-0493(1968)096<0617:HH>2.0.CO;2

Heng, J., Y. Wang, and W. Zhou, 2017: Revisiting the balanced and unbalanced aspects of tropical cyclone intensification. *J. Atmos. Sci.*, **74**, 2575–2591, https://doi.org/10.1175/JAS-D-17-0046.1.

Heng, J., Y. Wang, and W. Zhou, 2018: Reply to "Comments on 'Revisiting the balanced and unbalanced aspects of tropical cyclone intensification'". *J. Atmos. Sci.*, **75**, 2497–2505, https://doi.org/10.1175/JAS-D-18-0020.1.

Kepert, J., 2001: The dynamics of boundary layer jets within the tropical cyclone core. Part I: Linear theory. *J. Atmos. Sci.*, **58**, 2469–2484, https://doi.org/10.1175/1520-0469(2001)058<2469:TDOBLJ>2.0.CO;2.

Kepert, J., and Y. Wang, 2001: The dynamics of boundary layer jets within the tropical cyclone core. Part II: Nonlinear enhancement. *J. Atmos. Sci.*, **58**, 2485–2501, https://doi.org/10.1175/1520-0469(2001)058<2485:TDOBLJ>2.0.CO;2.

Kepert, J. D., 2006a: Observed boundary layer wind structure and balance in the hurricane core. Part I: Hurricane Georges. *J. Atmos. Sci.*, **63**, 2169–2193, https://doi.org/10.1175/JAS3745.1.

Kepert, J. D., 2006b: Observed boundary layer wind structure and balance in the hurricane core. Part II: Hurricane Mitch. *J. Atmos. Sci.*, **63**, 2194–2211, https://doi.org/10.1175/JAS3746.1.

Kepert, J. D., 2010a: Slab- and height-resolving models of the tropical cyclone boundary layer. Part I: Comparing the simulations. *Quart. J. Roy. Meteor. Soc.*, **136**, 1686–1699, https://doi.org/10.1002/qj.667.

Kepert, J. D., 2010b: Slab- and height-resolving models of the tropical cyclone boundary layer. Part II: Why the simulations differ. *Quart. J. Roy. Meteor. Soc.*, **136**, 1700–1711, https://doi.org/10.1002/qj.685.

Kepert, J. D., 2017: Time and space scales in the tropical cyclone boundary layer, and the location of the eyewall updraft. *J. Atmos. Sci.*, **74**, 3305–3323, https://doi.org/10.1175/JAS-D-17-0077.1.

Kuo, H.-L., 1959: Dynamics of convective vortices and eye formation. *The Atmospheric and Sea in Motion,* B. Bolin, Ed., Rockefeller Institute Press, 413–424.

Li, T.-H., and Y. Wang, 2020a: The role of boundary layer dynamics in tropical cyclone intensification. Part I: Sensitivity to surface drag coefficient. *J. Meteor. Soc. Japan*, **99** (2), https://doi.org/10.2151/jmsj.2021-027.

Li, T.-H., and Y. Wang, 2020b: The role of boundary layer dynamics in tropical cyclone intensification. Part II: Sensitivity to initial vortex structure. *J. Meteor. Soc. Japan*, **99** (2), https://doi.org/10.2151/jmsj.2021-028.

Li, Y., Y. Wang, and Y. Lin, 2019: Revisiting the dynamics of eyewall contraction of tropical cyclones. *J. Atmos. Sci.*, **76**, 3229–3245. https://doi.org/10.1175/JAS-D-19-0076.1.

Li, Y., Y. Wang, and Y. Lin, 2020: How much does the upward advection of the supergradient component of boundary layer wind contribute to tropical cyclone intensification and maximum intensity? *J. Atmos. Sci.*, **77**, 2649–2664, https://doi.org/10.1175/JAS-D-19-0350.1.

Li, Y.-L., Y. Wang, and Y.-L Lin, 2020: Reply to "Comments on 'How much does the upward advection of the supergradient component of boundary layer wind contribute to tropical cyclone intensification and maximum intensity?'". *J. Atmos. Sci.*, **77**, 4379–4384, https://doi.org/10.1175/JAS-D-20-0242. (in press).

Malkus, J. S., 1958: On the structure and maintenance of the mature hurricane eye. *J. Meteor.*, **15,** 337–349. https://doi.org/10.1175/1520-0469(1958)015<0337:OTSAMO>2.0.CO;2.

Mitsuta, Y., T. Suenobu, and T. Fujii, 1988: Supergradient surface wind in the eye of a typhoon. *J. Meteor. Soc. Japan*, **66**, 505–508.

Miyamoto, Y., M. Satoh, H. Tomita, K. Oouchi, Y. Yamada, C. Kodama, and J. Kinter III, 2014: Gradient wind balance in tropical cyclones in high-resolution global experiments. *J. Atmos. Sci.*, **142**, 1908–1926, https://doi.org/10.1175/MWR-D-13-00115.1

Montgomery, M. T. and R. K. Smith, 2017: Recent developments in the fluid dynamics of the tropical cyclones. *Ann. Rev. Fluid Mech.*, **49**, 541–574, https://doi.org/10.1146/annurev-fluid-010816- 060022.

Montgomery, M. T. and R. K. Smith, 2018: Comments on "Revisiting the balanced and unbalanced aspects of tropical cyclone intensification". *J. Atmos. Sci.*, **75**, 2491–2496, https://doi.org/10.1175/JAS-D-17-0323.1.

Rosenthal, S. L., 1962: A theoretical analysis of the field of motion in the hurricane boundary layer. National Hurricane Research Project Rep. 56, U.S. Dept. of Commerce, 12 pp.

Rotunno, R., 2014: Secondary circulations in rotating-flow boundary layers. *Aust. Meteor. Oceanogr. J.*, **64**, 27–35. http://www.bom.gov.au/amoj/docs/2014/rotunno_hres.pdf

Rotunno, R., and K. A. Emanuel, 1987: An air-sea interaction theory for tropical cyclones. Part II: Evolutionary study using a nonhydrostatic axisymmetric numerical model. *J. Atmos. Sci.*, **44**, 542–561, https://doi.org/10.1175/1520-0469(1987)044<0542:AAITFT>2.0.CO;2.

Rotunno, R., and G. H. Bryan, 2012: Effects of parameterized diffusion on simulated hurricanes. *J. Atmos. Sci.*, **69**, 2284–2299, https://doi.org/10.1175/JAS-D-11-0204.1.

Schwendike, J., and J. D. Kepert, 2008: The boundary layer winds in Hurricanes Danielle (1998) and Isabel (2003). *Mon. Wea. Rev.*, **136**, 3168–3192, https://doi.org/10.1175/2007MWR2296.1

Schmidt, C. W. and R. K. Smith, 2016: Tropical cyclone evolution in a minimal axisymmetric model revisited. *Quart. J. Roy. Meteor. Soc.*, **142**, 1505–1516, https://doi.org/10.1002/qj.2753.

Shapiro, L. J., 1983: The asymmetric boundary layer under a translating hurricane. *J. Atmos. Sci.*, **40**, 1984–1998, https://doi.org/10.1175/1520-0469(1983)040<1984:TABLFU>2.0.CO;2

Stern, D. P., J. D. Kepert, G. H. Bryan, and J. D. Doyle, 2020: Understanding atypical midlevel wind speed maxima in hurricane eyewalls. *J. Atmos. Sci.*, **77**, 1531–1557, https://doi.org/10.1175/JAS-D-19-0191.1.

Thompson, G., P. R. Field, R. M. Rasmussen, and W. D. Hall, 2008: Explicit forecasts of winter precipitation using an improved bulk microphysics scheme. Part II: Implementation of a new snow parameterization. *Mon. Wea. Rev.*, **136**, 5095–5115, https://doi.org/10.1175/2008MWR2387.1.

Williams, G. J., 2015: The effects of vortex structure and vortex translation on the tropical cyclone boundary layer wind field. *J. Adv. Model. Earth Syst.*, **7**, 188–214, https://doi.org/10.1002/2013MS000299.

Willoughby, H. E., 1990: Gradient balance in tropical cyclones. *J. Atmos. Sci.*, **47**, 265–274, https://doi.org/10.1175/1520-0469(1990)047<0265:GBITC>2.0.CO;2

Willoughby, H. E., 1991: Reply. *J. Atmos. Sci.,* **48,** 1209–1212, https://doi.org/10.1175/1520-0469(1991)048<1209:R>2.0.CO;2

Wood, V. T., and L. W. White, 2011: A new parametric model of vortex tangential-wind profiles: Development, testing, and verification. *J. Atmos. Sci.*, **68**, 990–1006, https://doi.org/10.1175/2011JAS3588.1.

Xu, J., and Y. Wang, 2018: Effect of initial vortex structure on intensification of a numerically simulated tropical cyclone. *J. Meteor. Soc. Japan*, **96**, 111–126, https://doi.org/10.2151/jmsj.2018-014.

Zhang, D.-L., Y. Liu, and M. K. Yau, 2001: A multiscale numerical study of Hurricane Andrew (1992). Part IV: Unbalanced flows. *Month. Wea. Rev*., **129**, 92–107, https://doi.org/10.1175/1520-0493(2001)129<0092:AMNSOH>2.0.CO;2

Zhang, J. A., and M. T. Montgomery, 2012: Observational estimates of the horizontal eddy diffusivity and mixing length in the low-level region of intense hurricanes, *J. Atmos. Sci.*, **69**, 1306–1316, https://doi.org/10.1175/JAS-D-11-0180.1.

Zhang, J. A., F. D. Marks, M. T. Montgomery, and S. Lorsolo, 2011, An estimation of turbulent characteristics in the low-level region of intense Hurricanes Allen (1980) and Hugo (1989), *Mon. Wea. Rev.*, **139**, 1447–1462. https://doi.org/10.1175/2010MWR3435.1

Table 1. List of numerical experiments.

TCBL model exp.	Vertical advection of horizontal wind	Initial gradient wind
CTL_BL	Default model settings	Gradient wind profile at 2-km height from CTL_CM1
noU_BL	Set $-w\,\partial u/\partial z = 0$ if $r \le 40$ km	
noVa_BL	Set $-w\,\partial v/\partial z = -w\,\partial v_g/\partial z$ if $r \le 40$ km	
noUVa_BL	Set $-w\,\partial v/\partial z = -w\,\partial v_g/\partial z$ & $-w\,\partial u/\partial z = 0$ if $r \le 40$ km	
CTL_2d_BL	Default model settings as in CTL_BL	2D gradient wind field from CTL_CM1
noU_2d_BL	Same as noU_BL	2D gradient wind field from noU_CM1
noVa_2d_BL	Same as noVa_BL	2D gradient wind field from noVa_CM1
noUVa_2d_BL	Same as noUVa_BL	2D gradient wind field from noUVa_CM1

CM1 exp.	Vertical advection of horizontal wind	Initial gradient wind
CTL_CM1	Default model settings	Using Analytical vortex profile according to Wood and White (2011) with maximum wind speed of 15 m s^{-1} at a radius of 80 km and radial shape parameter of 1.6
noU_CM1	Set $-w\,\partial u/\partial z$=0 if $r \le 40$ km, $z \le 3$ km, and $t \ge 48$ h	
noVa_CM1	Set $-w\,\partial v/\partial z$=$-w\,\partial v_g/\partial z$ if $r \le 40$ km, $z \le 3$ km, and $t \ge 48$ h	
noUVa_CM1	Set $-w\,\partial u/\partial z$ =0 & $-w\,\partial v/\partial z$ = $-w\,\partial v_g/\partial z$ if $r \le 40$ km, $z \le 3$ km, and $t \ge 48$ h	

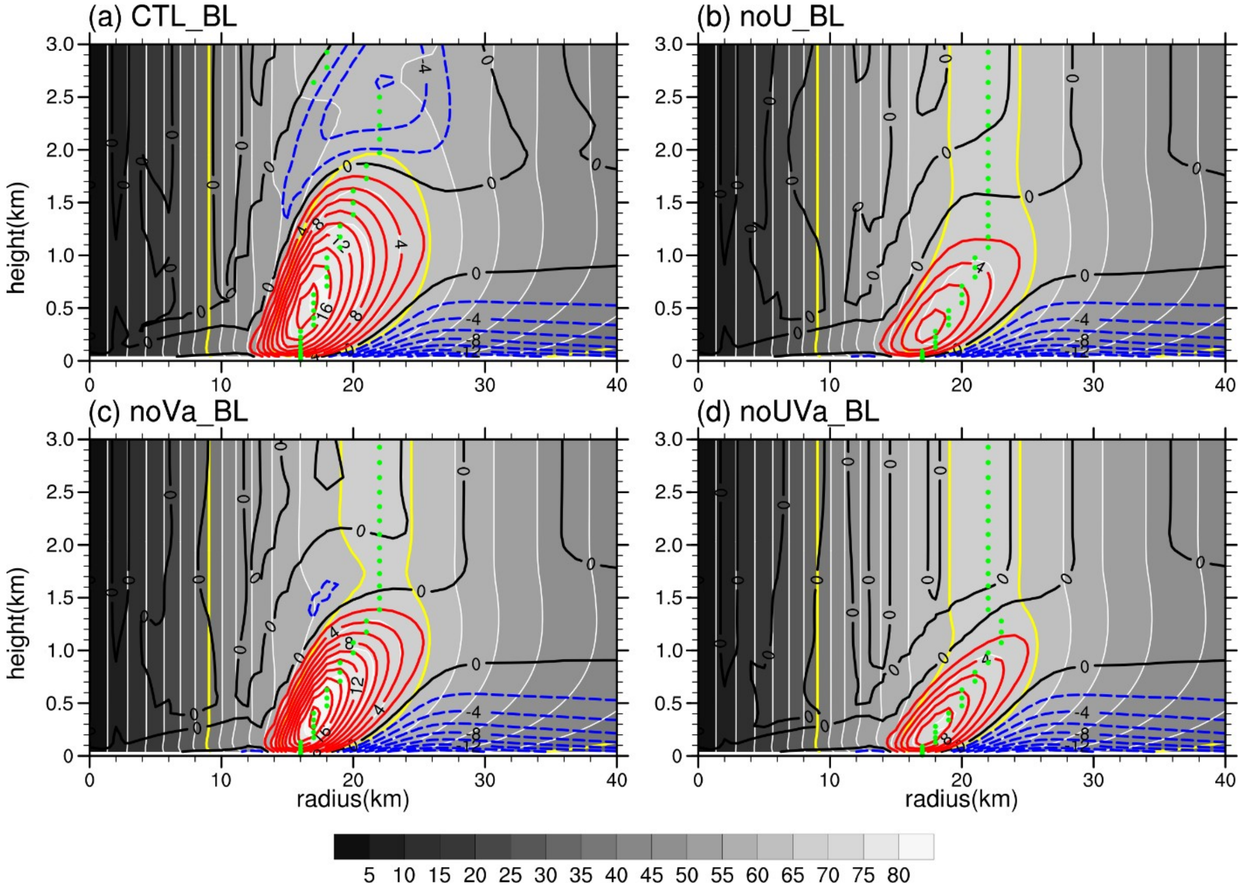

FIG. 1. Radius-height cross sections of total tangential wind (shaded; the 35 and 65 m s^{-1} contours are highlighted in yellow) and agradient wind (with contour interval of 2 m s^{-1}, red for positive, blue for negative, and black for zero) in the steady-state response in (a) CTL_BL, (b) noU_BL, (c) noVa_BL, and (d) noUVa_BL. The green dots mark the radial location of the maximum wind speed at each level.

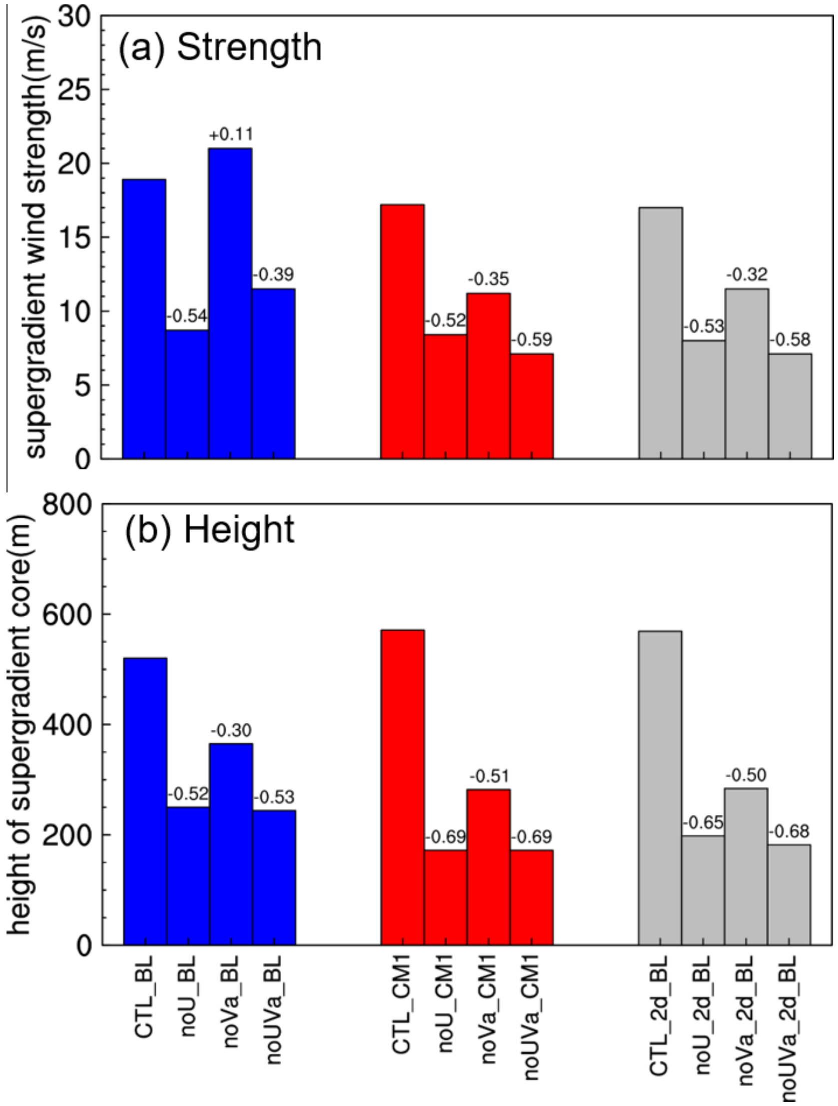

FIG. 2. Bar plots of the strength (a) and height (b) of the supergradient wind core in the three sets of experiements listed in Table 1, including those from the TCBL model forced by the height-independent gradient wind at 2-km height from the average in the quasi-steady stage during 96–120 h of simulation in CTL_CM1 (blue), those from CM1 experiments (red), and those from the TCBL model forced by the two-dimentional gradient wind from the corresponding CM1 experiments (grey). The numbers on the top of the bars denote the change ratios of sensitivity experiments compared to the corresponding control experiment. Red and grey bars will be discussed in section 4.

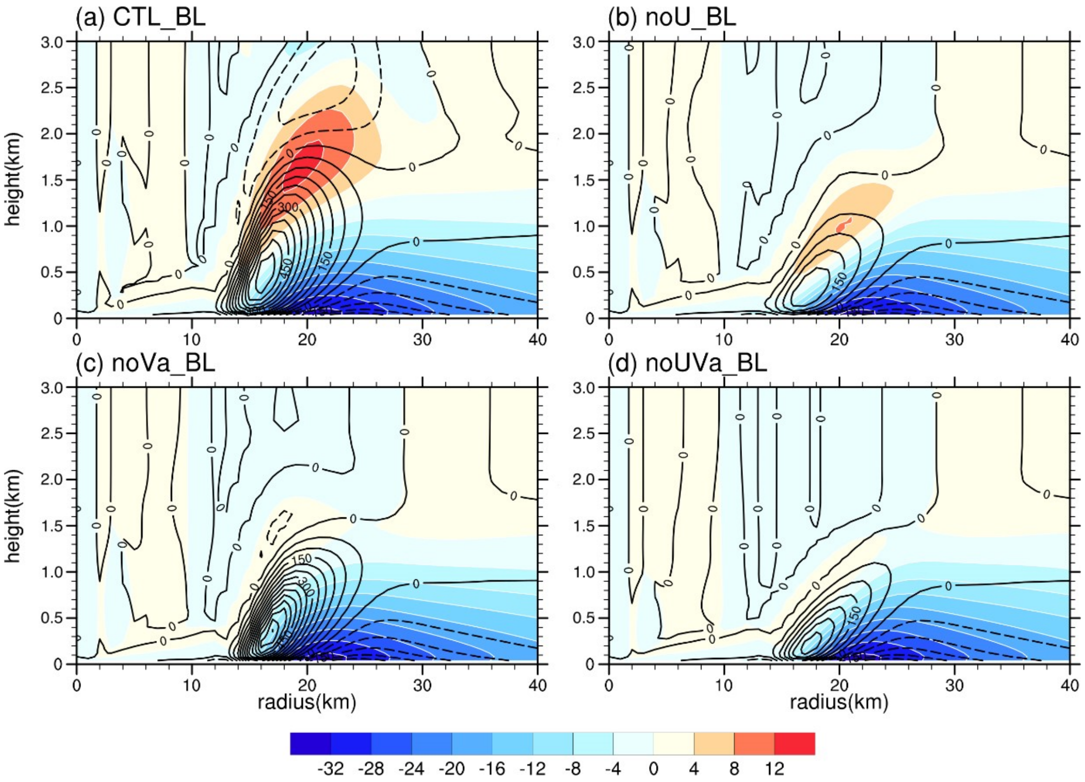

FIG. 3. Radius-height cross sections of radial wind (shaded, m s^{-1}) and agradient force (with contour interval of 50 m s^{-1} hr^{-1}, solid for positive and dashed for negative values) in the steady state response in (a) CTL_BL, (b) noU_BL, (c) noVa_BL, and (d) noUVa_BL.

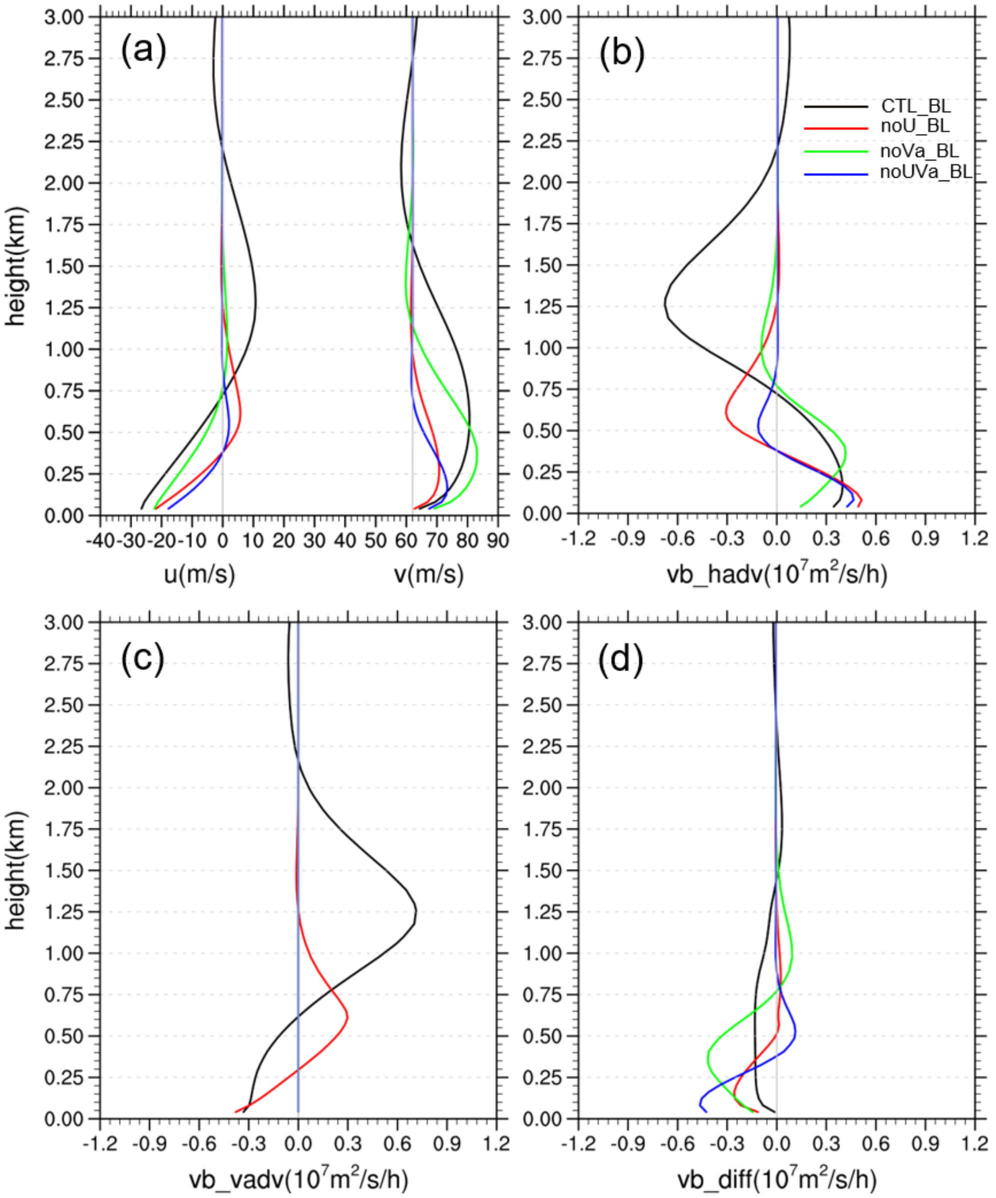

FIG. 4. Vertical profiles of tangential and radial wind speeds (a) and AAM budget components due to (b) horizontal advection (vb_hadv), (c) vertical advection (vb_vadv) and (d) diffusion (vb_diff) at 17-km radius (near the radius of maximum supergradient wind speed in CTL_BL) in CTL_BL (black), noU_BL (red), noVa_BL (green), and noUVa_BL (blue). The two grey vertical lines in (a) represent zero radial wind and gradient wind speed, respectively.

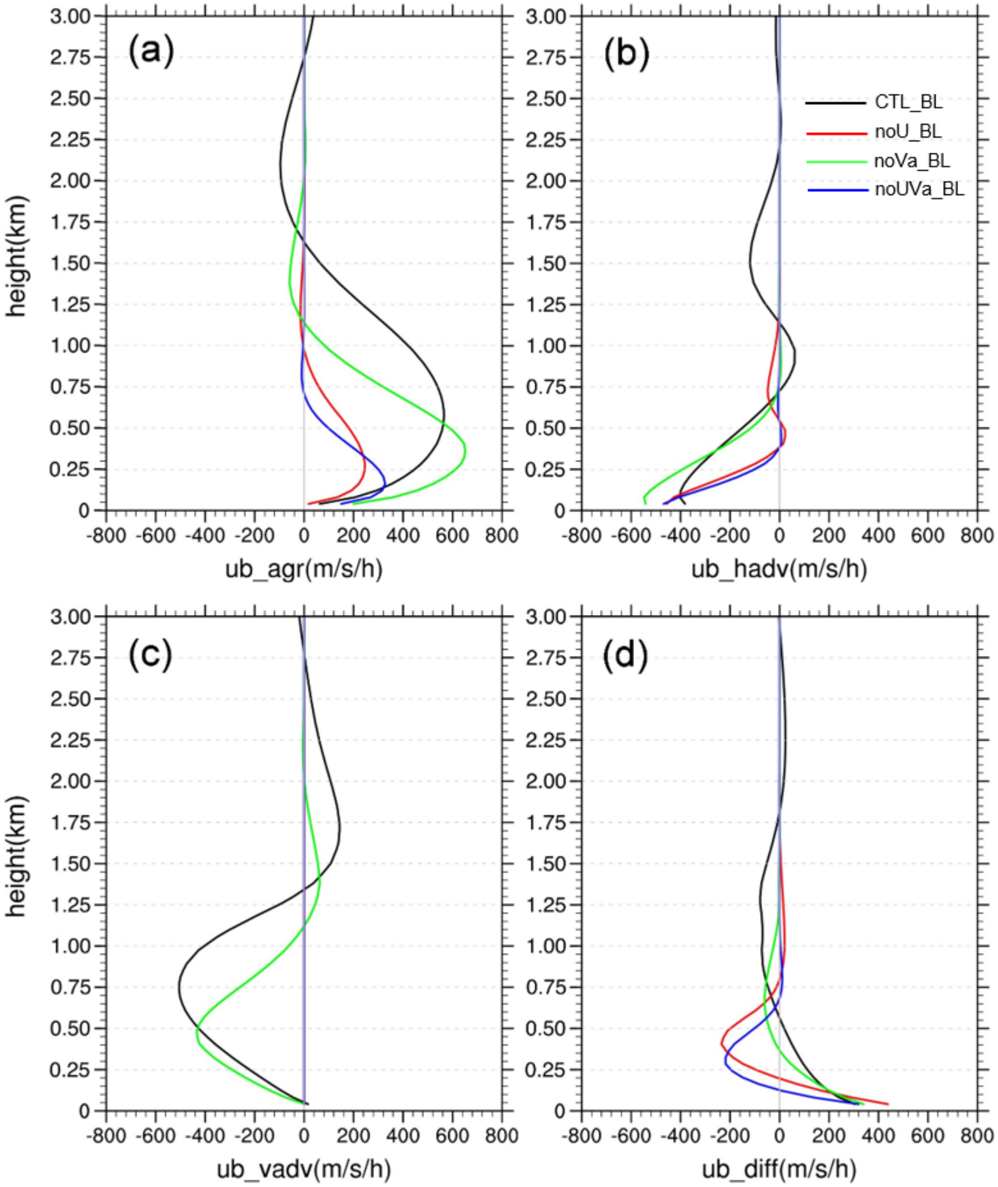

FIG. 5. Vertical profiles of radial wind budgets at 17-km radius in CTL_BL (black), noU_BL (red), noVa_BL (green), and noUVa_BL (blue). The budget components include (a) agradient force (ub_agr), (b) horizontal advection (ub_vadv), (c) vertical advection (ub_vadv), and (d) diffusion (ub_diff).

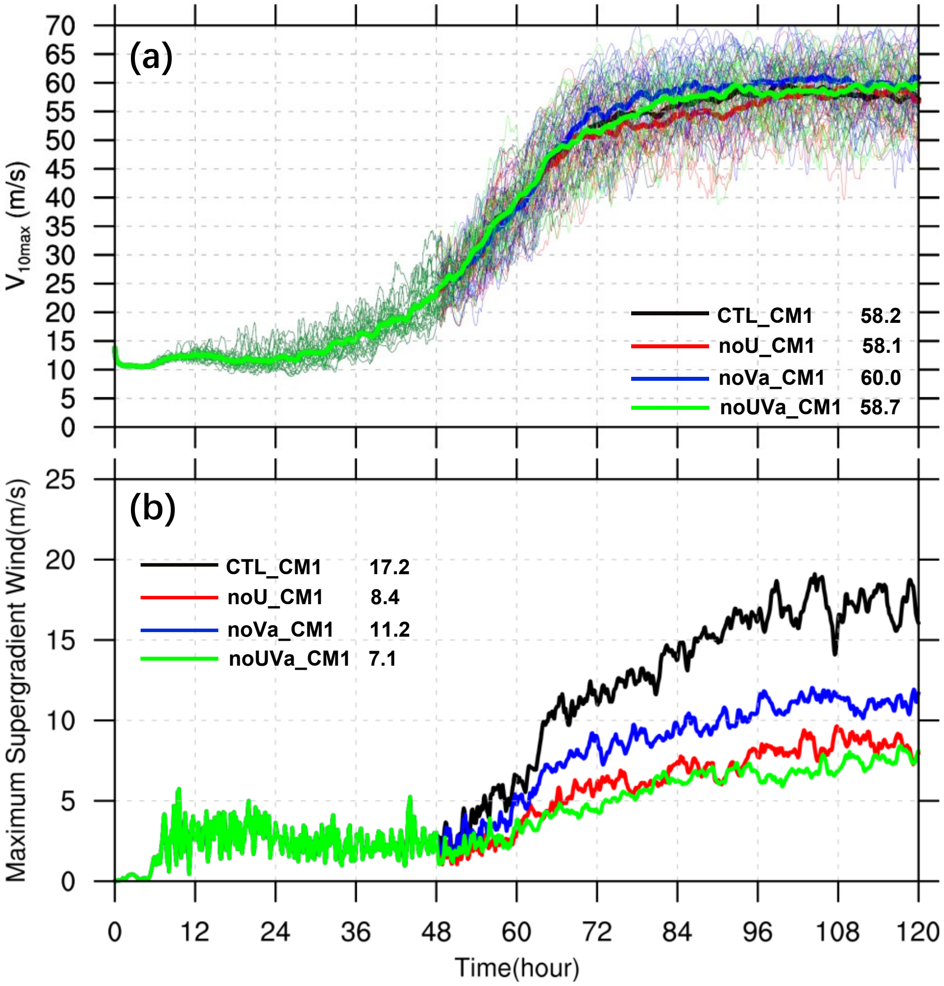

FIG. 6. Time series of (a) maximum 10-m tangential wind speed and (b) maximum supergradient wind speed in CTL_CM1 (black), noU_CM1 (red), noVa_CM1 (blue), and noUVa_CM1 (green), with the thick curves showing the ensemble mean and the thin curves showing the 21 individual members for the corresponding experiments in (a). The values in panels (a) and (b) refer to the averaged maximum 10-m height tangential wind speed and maximum supergradient wind speed during the quasi-steady stage (96-120 h of simulations), respectively.

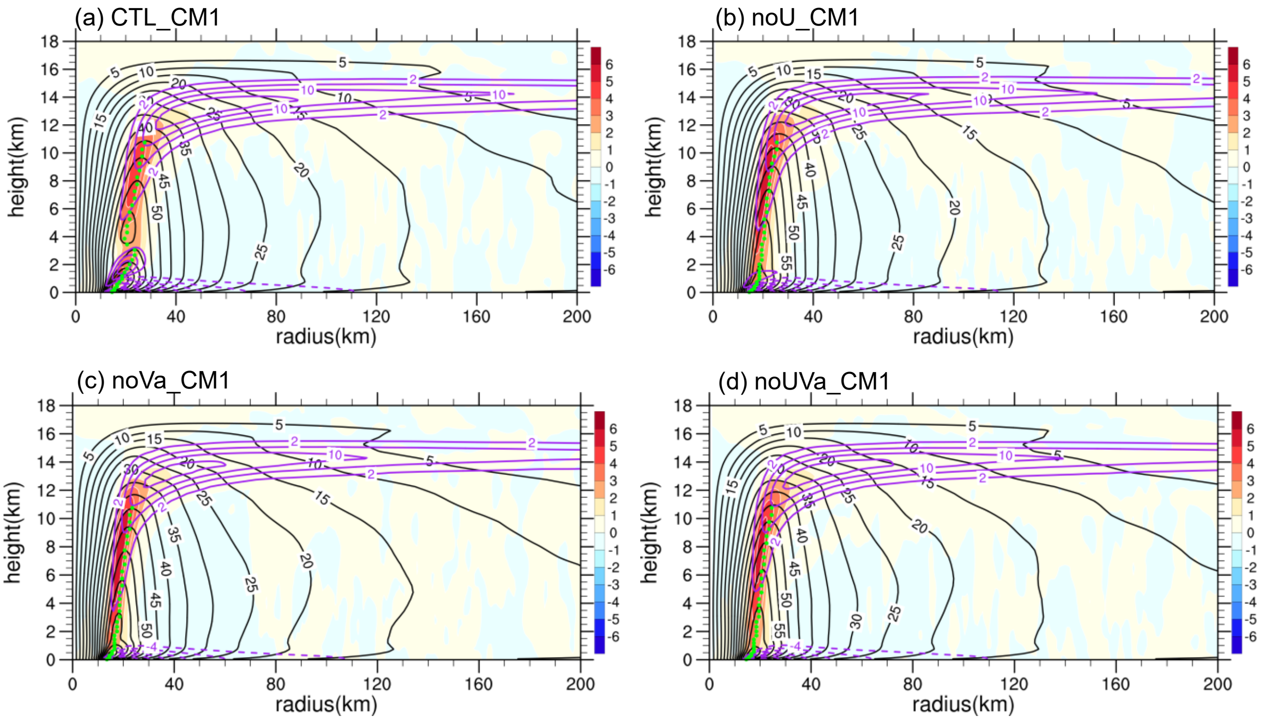

FIG. 7. The radial-vertical structures of the simulated TCs in CTL_CM1 (a), noU_CM1 (b), noVa_CM1 (c), and noUVa_CM1 (d), respectively, averaged in the quasi-steady stage during 96-120 h of simulations. The black and purple contours and shades are for ensemble mean tangential and radial winds (m s^{-1}), and vertical motion (m s^{-1}), respectively.

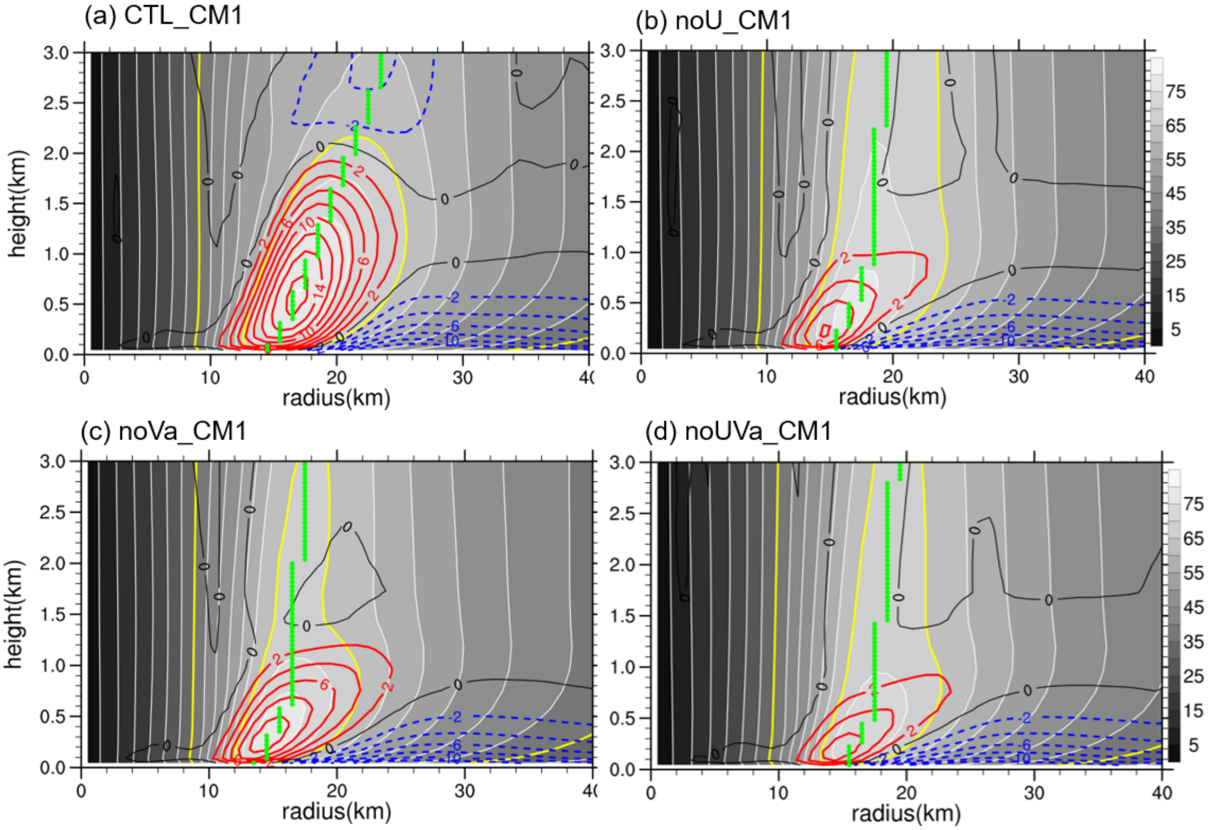

FIG. 8. Same as Fig. 1 but for the results from the quasi-steady stage averaged during 96-120 h in CTL_CM1 (a), noU_CM1 (b), noVa_CM1 (c), and noUVa_CM1 (d), respectively.

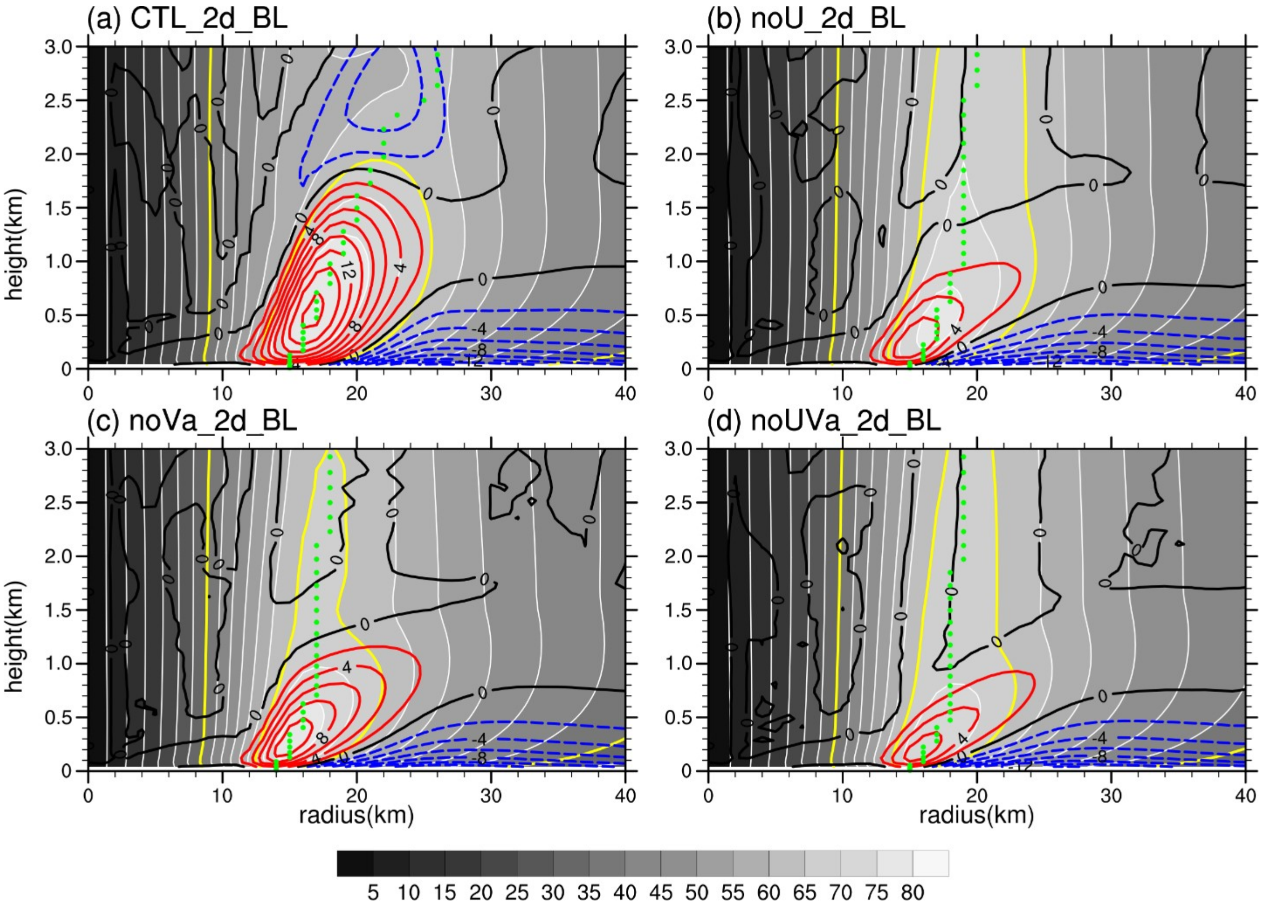

FIG. 9. Same as Fig. 1 but for results from the four extra experiments (CTL_2d_BL [a], noU_2d_BL [b], noVa_2d_BL [c], and noUVa_2d_BL [d]) in the TCBL model forced by the two-dimentional pressure gradient force from the corresponding experiments in CM1.

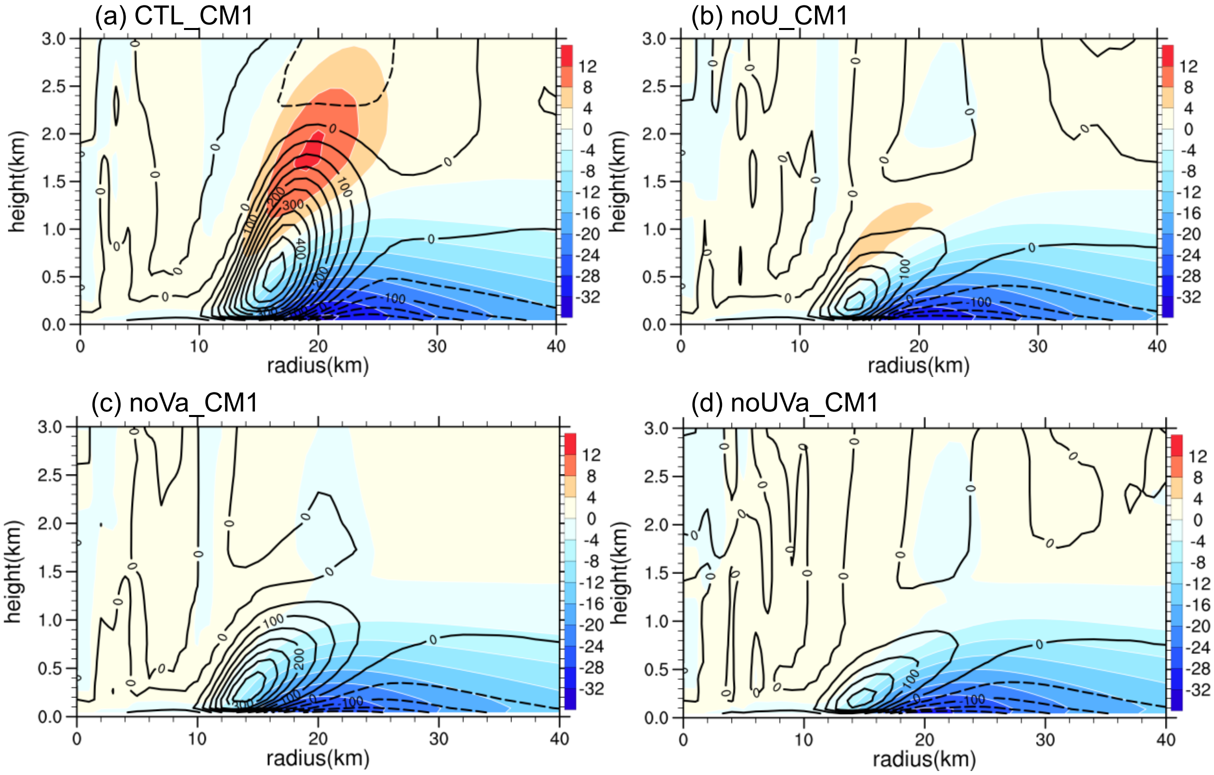

FIG. 10. Same as Fig. 3 but for the results from the quasi-steady stage averaged during 96-120 h in CTL_CM1 (a), noU_CM1 (b), noVa_CM1 (c), and noUVa_CM1 (d), respectively.

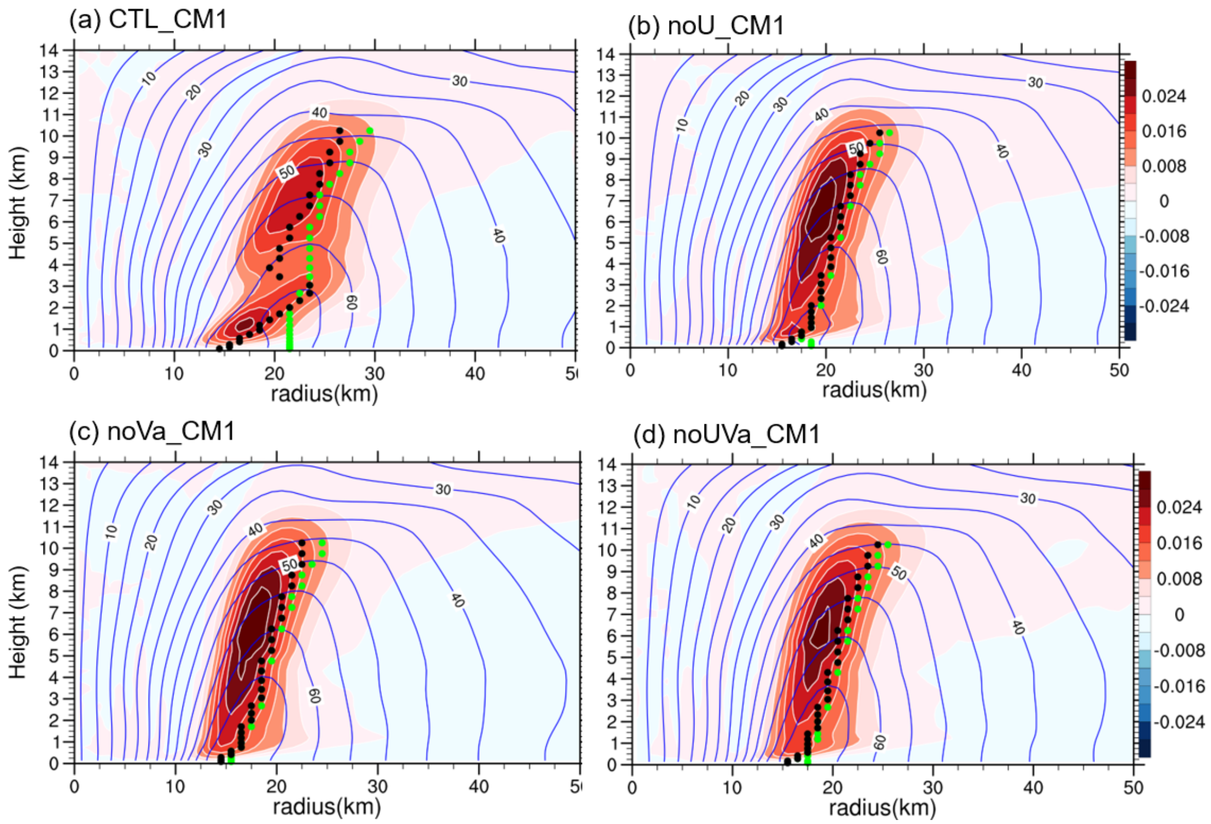

FIG. 11. Radius-height cross sections of the ensemble mean diabatic heating rate (shaded, K s^{-1}) and gradient wind speed (contours, m s^{-1}) in CTL_CM1 (a), noU_CM1 (b), noVa_CM1 (c), and noUVa_CM1 (d), respectively, averaged in the quasi-steady stage during 96-120 h of simulations. The black dots mark the radial location of maximum total tangential wind and the green dots mark the radial location of maximum gradient wind speed at each level.